Structural and Electrochemical Studies of Rhombohedral $Na_2TiM(PO_4)_3$ and $Li_{1.6}Na_{0.4}TiM(PO_4)_3$ (M = Fe, Cr) Phosphates

Sébastien Patoux,[†] Gwenaëlle Rousse,[‡] Jean-Bernard Leriche,[†] and Christian Masquelier*,[†]

Laboratoire de Réactivité et de Chimie des Solides, CNRS UMR 6007, Université de Picardie Jules Verne, 33 rue Saint-Leu, 80039 Amiens Cedex, France, Institut Laue Langevin, BP 156, F-38042, Grenoble Cedex 9, France, and Laboratoire de Physique des Milieux Condensés, Université Pierre et Marie Curie, 4, place Jussieu, 75252 Paris Cedex 05, France

Received December 19, 2002. Revised Manuscript Received March 14, 2003

The crystal structures of NASICON compositions $Z_2TiM(PO_4)_3$ (Z = Na, Li; M = Cr, Fe) were investigated through powder neutron diffraction on the beam lines D1A (λ = 1.9104 Å) and D2B (λ = 1.5924 Å) at ILL, Grenoble, France. $Na_2TiCr(PO_4)_3$ and $Na_2TiFe(PO_4)_3$ are isostructural. They crystallize in the space group $R\bar{3}c$, with the sodium ions being located in the M1 ($\tau \sim 1$) and M2 sites ($\tau \sim 1/3$). NASICON $Li_{1.6}Na_{0.4}TiCr(PO_4)_3$ and $Li_{1.6}Na_{0.4}TiFe(PO_4)_3$ were prepared through ion exchange from the sodium analogues. They crystallize in the space group $R\bar{3}$, with the lithium ions being located in the M3 tetrahedral site. The remaining, unexchanged, sodium ions are still located on the M1 site. Electrochemical insertion of sodium or lithium into these structures was followed through slow intermittent titration techniques coupled with *in situ* X-ray diffraction. We show that for both $Na_{2+x}TiM(PO_4)_3$ and $Li_{1.6+x}Na_{0.4}TiM(PO_4)_3$ ($0 \le x \le 1$ for M = Cr, $0 \le x \le 2$ for M = Fe), the insertion proceeds through a single-phase mechanism.

Introduction

Since the works of Padhi et al.,[1−7] 3-D open frameworks built on polyanions such as tetrahedral XO_4^{n-} groups (X = P, Mo, W, S) are considered as possible alternatives for a new generation of positive electrodes for lithium batteries. Among these 3-D structures, NASICON compositions were extensively studied for their structural stability and fast ion conduction; as solid electrolytes in the early days, as chemical sensors, or more recently as insertion electrodes.

Besides the well-documented NASICON $ZTi_2(PO_4)_3$ and $Z_3M_2(PO_4)_3$ (M = Fe, Cr; Z = Li, Na) compositions, mixed Ti/M phosphates $Z_2TiM(PO_4)_3$ (Ti^{IV}, M^{III}) have been the object of limited work so far apart from a first report on the preparation of B−$Na_2TiM(PO_4)_3$ by Perret[8] and on sodium insertion into $Na_2TiFe(PO_4)_3$ by Tillement.[9] A preliminary electrochemical investigation of NASICON $Li_2TiFe(PO_4)_3$ was reported more recently by Goodenough's group.[5,10]

Depending on the preparation procedure, $Li_2TiM(PO_4)_3$ (M = Fe, Cr) can adopt another crystalline form, noted "A" (space group *Pbna*), releated to that of $Sc_2(WO_4)_3$.[11] A detailed structural and electrochemical study of orthorhombic $Li_2TiM(PO_4)_3$ is given in ref 12. In this paper, we present the crystal structures of NASICON (noted "B") $Z_2TiFe(PO_4)_3$ and $Z_2TiCr(PO_4)_3$ (Z = Na, Li) solved by Rietveld refinements of neutron powder diffraction patterns. Electrochemical sodium and lithium insertions into the four materials are presented using slow electrochemical titration techniques (GITT, PITT) and *in situ* X-ray diffraction.

Experimental Section

TiO_2, M_2O_3 (M = Fe, Cr), $NH_4H_2PO_4$, and NaH_2PO_4 were intimately mixed in stoichiometric proportions. After intermediate thermal treatments and grindings, pure B−$Na_2TiFe(PO_4)_3$ (B−NTFP) and B−$Na_2TiCr(PO_4)_3$ (B−NTCP) powders were obtained by solid-state reaction with a final treatment

* To whom correspondence should be addressed. E-mail: christian.masquelier@sc.u-picardie.fr.
† Université de Picardie Jules Verne.
‡ Institut Laue Langevin, and Laboratoire de Physique des Milieux Condensés, Université Pierre et Marie Curie.

(1) Padhi, A. K. Ph.D. Thesis, The University of Texas at Austin, 1997.
(2) Nanjundaswamy, K. S.; Padhi, A. K.; Goodenough, J. B.; Okada, S.; Ohtsuka, H.; Arai, H.; Yamaki, J. *Solid State Ionics* **1996**, *92*, 1−10.
(3) Padhi, A. K.; Nanjundaswamy, K. S.; Goodenough, J. B. *J. Electrochem. Soc.* **1997**, *144*, 1188−1194.
(4) Padhi, A. K.; Nanjundaswamy, K. S.; Masquelier, C.; Okada, S.; Goodenough, J. B. *J. Electrochem. Soc.* **1997**, *144*, 1609−1613.
(5) Padhi, A. K.; Nanjundaswamy, K. S.; Masquelier, C.; Goodenough, J. B. *J. Electrochem. Soc.* **1997**, *144*, 2581−2586.
(6) Padhi, A. K.; Manivannan, V.; Goodenough, J. B. *J. Electrochem. Soc.* **1998**, *145*, 1518−1520.
(7) Masquelier, C.; Padhi, A. K.; Nanjundaswamy, K. S.; Goodenough, J. B. *J. Solid State Chem.* **1998**, *135*, 228−234.
(8) Perret, R. *J. Less Common Metals* **1988**, *144*, 195−200.
(9) Tillement, O.; Angenault, J.; Couturier, J. C.; Quarton, M. *Solid State Ionics* **1992**, *53−56*, 391−399.
(10) Goodenough, J. B.; Manivannan, V. *Denki Kagaku* **1998**, *66*, 1173−1181.
(11) Abrahams, S. C.; Bernstein, J. L. *J. Chem. Physics* **1966**, *45*, 2745−2750.
(12) Patoux, S.; Rousse, G.; Leriche, J.-B.; Masquelier, C. *Chem. Mater.* submitted for publication.

10.1021/cm020479p CCC: $25.00
Published on Web 04/24/2003

Table 1. Lattice Constants and Rietveld Refinement Results from Neutron Diffraction (at ILL, Grenoble, France) with λ = 1.9104 Å (D1A) or λ = 1.5924 Å (D2B), for B−$Na_2TiM(PO_4)_3$ and B−$Li_{1.6}Na_{0.4}TiM(PO_4)_3$ (M = Fe, Cr) at 300 K

composition	B−$Na_2TiFe(PO_4)_3$	B−$Li_{1.6}Na_{0.4}TiFe(PO_4)_3$	B−$Na_2TiCr(PO_4)_3$	B− $Li_{1.6}Na_{0.4}TiCr(PO_4)_3$
abbreviation	B−NTFP	B−LTFP	B−NTCP	B−LTCP
temperature (K)	300	300	300	300
instrument (at ILL, Grenoble, France)	D1A	D2B	D1A	D1A
wavelength (Å)	1.9104	1.5924	1.9104	1.9104
space group (No.)	$R\bar{3}c$ (167)	$R\bar{3}$ (148)	$R\bar{3}c$ (167)	$R\bar{3}$ (148)
a (Å)	8.603(1)	8.390(1)	8.563(1)	8.342(1)
b (Å)	8.603(1)	8.390(1)	8.563(1)	8.342(1)
c (Å)	21.713(1)	22.040(3)	21.684(1)	21.951(2)
c/a	2.524	2.627	2.532	2.631
V (Å^3)	1392(1)	1344(1)	1377(1)	1323(1)
Z	6	6	6	6
d (g·cm^{-3})	3.111	3.032	3.117	3.051
melting point (K)	1273(5)	1363(5)	1603(5)	1673(5)
number of independent reflections	178	597	186	330
number of global-refined parameters	1	1	1	1
number of profile-refined parameters	10	10	10	10
number of intensity-dependent parameters	19	35	14	24
R_p (%)	5.53	3.69	6.05	6.87
R_{wp} (%)	6.70	4.78	7.76	9.02
R_{exp} (%)	4.23	2.84	3.34	3.96
χ^2	2.51	2.85	5.40	5.18
R_{Bragg}	6.25	9.78	7.71	10.8
R_f	4.61	8.42	5.53	7.41

at 1203 K. Concerning the lithium counterparts, high-temperature solid-state reaction led to orthorhombic A−$Li_2TiM(PO_4)_3$ (M = Fe, Cr) ($Sc_2(WO_4)_3$-type), as observed for $Li_3Fe_2(PO_4)_3$.[13,14] Rhombohedral B−$Li_2TiM(PO_4)_3$ (M = Fe, Cr) (B−LTFP and B−LTCP) were obtained from B−$Na_2TiM(PO_4)_3$ (M = Fe, Cr) after three successive ion exchanges in molten $LiNO_3$. To favor ion exchanges, the molar ratio $Li_{LiNO_3}/Na_{NASICON}$ was set to > 20, and the mixtures were maintained for 2 h at 573 K. The final ion-exchanged solid was washed repeatedly with distilled water to eliminate the accompanying (Li,Na)NO_3 before drying overnight at 333 K. Chemical analysis indicated (Ti, M)/P ratio of 2/3, as expected. Importantly, chemical analysis also revealed that the $Na^+ \leftrightarrow Li^+$ ion-exchange from both NASICON $Na_2TiCr(PO_4)_3$ and $Na_2TiFe(PO_4)_3$ was not complete: the final product presented the formula $Li_{1.6}Na_{0.4}TiM(PO_4)_3$ (M = Fe, Cr).

Phase purities and lattice parameters determinations were carefully monitored by X-ray diffraction on either a Philips PW1710 diffractometer (Cu Kα radiation, $\theta-2\theta$ geometry, back monochromator) or a D8 Bruker diffractometer (Co Kα radiation, $\theta-\theta$ geometry, back monochromator). The experimental X-ray diffractograms are gathered in Figure 1. A list of lattice parameters and space groups of the four materials investigated is given in Table 1. The crystal structures were determined from neutron powder diffraction patterns recorded at 300 K on the high-resolution powder diffractometers D1A and D2B at ILL, Grenoble, France. Data collection with high direct space resolution (λ = 1.9104 and 1.5924 Å, Q_{max} = 6.5 Å^{-1} and 7.8 Å^{-1}, respectively) allowed a precise determination of the nuclear crystal structures. The program Fullprof[15] was used for structure refinements by using the Rietveld method.[16] For *in situ* X-ray diffraction, a Swagelok-type cell similar to the one described elsewhere[17] was horizontally mounted on the D8 Bruker diffractometer (Co Kα radiation, $\theta-\theta$ geometry, PSD counter).

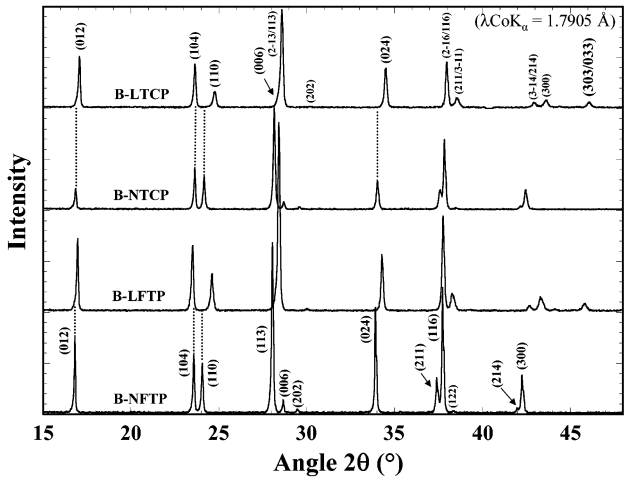

Figure 1. X-ray diffraction patterns collected at 300 K on a D8 Bruker diffractometer (Co Kα radiation, λ = 1.7905 Å, $\theta-\theta$ geometry, back monochromator) of B−$Na_2TiM(PO_4)_3$ ($R\bar{3}c$, noted B−NTMP) and B−$Li_{1.6}Na_{0.4}TiM(PO_4)_3$ ($R\bar{3}$, noted B−LTMP) (M = Fe, Cr).

Electrochemical lithium and sodium insertions were undertaken in standard Swagelok cell configuration with a lithium or sodium foil as the negative electrode and the active materials (AM) as positive electrode. The separator used was a Whatman GF/D borosilicate glass fiber sheet saturated with a 1 mol/L $LiPF_6$ electrolyte solution in EC/DMC (1:1 in weight), or 1 mol/L $NaClO_4$ in PC. For optimal electrochemical activity, the AM powders were initially mixed with Super P carbon (MMM Carbon, Belgium) by ball-milling in a SPEX 8000 mixer that generates energetic shocks between particles (250 mg of AM + 50 mg of SP, stainless steel ball of 4 g, 30 min). A "Mac-Pile" automatic cycling/data recording system (Biologic SA, Claix, France) operating either in galvanostatic or potentiostatic mode, was used for the data collecting. Standard electrode investigation was conducted at a galvanostatic regime of C/10 (one electron exchanged in 10 h). Galvanostatic intermittent titration technique (GITT) measurements consisted of 30-min charges or discharges at C/20 rate with open circuit periods of 30 min. Potentiostatic intermittent titration

(13) d'Yvoire, F.; Pintard-Srépel, M.; Bretey, E.; de la Rochère, M. *Solid State Ionics* **1983**, *9&10*, 851−858.
(14) Patoux, S.; Wurm, C.; Morcrette, M.; Rousse, G.; Masquelier, C. *J. Power Sources*, in press.
(15) Rodriguez-Carvajal, J. *Physica B* **1993**, *192*, 55. http://www.llb.cea.fr/fullweb/powder.htm.
(16) Rietveld, H. M. *J. Appl. Crystallogr.* **1969**, *2*, 65.
(17) Patoux, S.; Masquelier, C. *Chem. Mater.* **2002**, *14*, 2334−2341.

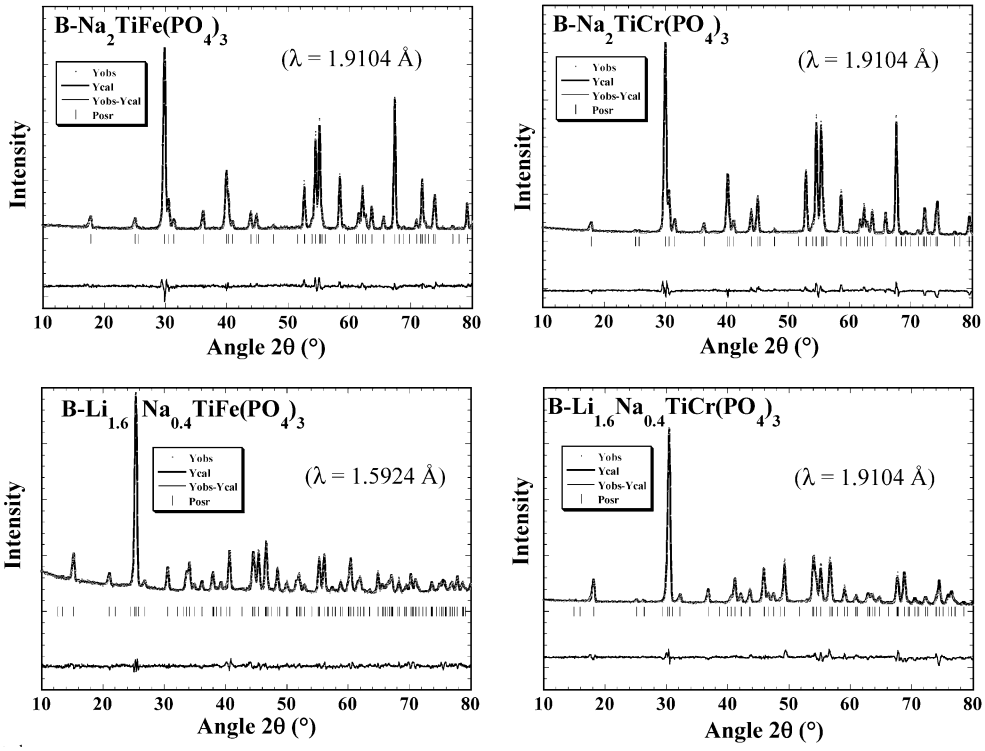

Figure 2. Neutron diffraction profiles of experimental (circles) and calculated (full lines) patterns refined by the Rietveld method for B−$Na_2TiM(PO_4)_3$ ($R\bar{3}c$) and B−$Li_{1.6}Na_{0.4}TiM(PO_4)_3$ ($R\bar{3}$) (M = Fe, Cr). Data collected at 300 K (ILL Grenoble, France, on D1A (λ = 1.9104 Å) and D2B (λ = 1.5840 Å)). The vertical lines indicate the possible Bragg positions.

technique (PITT) measurements were conducted using potential steps of 10 mV limited by a minimum current equivalent to a C/300 regime. For *in situ* X-ray diffraction, GITT charge and discharge were conducted at a C/10 regime interrupted every hour by relax periods during which each pattern was recorded.

Results and Discussions

1. Crystal Structures of NASICON $Na_2TiM(PO_4)_3$ (M = Fe, Cr). Both $Na_2TiCr(PO_4)_3$ (a = 8.563(1) Å and c = 21.684(1) Å) and $Na_2TiFe(PO_4)_3$ (a = 8.603(1) Å and c = 21.713(1) Å) adopt the NASICON structure in the space group $R\bar{3}c$, with similar c/a ratio (Table 1), in agreement with the data of Perret.[8] A larger lattice volume for M = Fe than for M = Cr may be the consequence of the slight difference in ionic radii between Fe^{3+} (0.645 Å) and Cr^{3+} (0.615 Å) in octahedral environments.[18] The fact that all the diffraction peaks in both neutron and X-ray diffraction data are indexed in the "original" NASICON cell in the space group $R\bar{3}c$ implies that no long range ordering takes place between Ti and Cr or Fe. Hence, the single octahedral M site (*12c*) of the NASICON framework is statistically equally occupied by (Ti, Fe) or (Ti, Cr). Rietveld refinements were conducted using a pseudo-Voigt profile function with asymmetry correction for angles below 50.0 2θ (°). The list of atomic coordinates of the high-temperature form (γ) of $Na_3Fe_2(PO_4)_3$[19] was used as the starting model, with Na(1) (*6b*) and Na(2) (*18e*) occupation rates constrained to 1 and $^1/_3$ in the early stages of refinement, respectively. Experimental and calculated patterns are given in Figure 2. Lists of atomic coordinates and thermal displacement factors are given in Table 2a and b. Selected interatomic distances are reported in Table 3a.

In the case of B−$Na_2TiFe(PO_4)_3$, the accurate occupation rates are 0.98(1) and 0.34(1) for Na(1) (M1) and Na(2) (M2), respectively (Table 2a). The thermal displacement factors for the sodium ions were refined anisotropically and showed stronger displacements in the (**a**, **b**) plane than along the **c**-axis, as usually observed for NASICON compositions (Figure 3). The neutron scattering lengths of titanium (−0.3438) and chromium (0.3835) are opposite, and necessitated the use of constraints to the refinement of the structure of B−$Na_2TiCr(PO_4)_3$. Accordingly, the isotropic thermal displacement parameters of Cr and Ti were not refined, but were fixed at 0.7 (Table 2b). Similarly to B−$Na_2TiFe(PO_4)_3$, the occupation rates of M1 and M2 are 0.96(1) and 0.35(1), respectively. The same behavior concerning the anisotropic thermal displacement factors of Na(1) was also encountered, that is β_{11} (= β_{22}) $\gg \beta_{33}$. Bond lengths (Table 3a), angles, bond valence sums, and polyhedra distortions of both materials were calculated and gave very consistent values, confirming the validity of the structures.

2. Crystal Structures of NASICON $Li_{1.6}Na_{0.4}TiM(PO_4)_3$ (M = Fe, Cr). The compositions deduced from the chemical analysis correspond approximately to the formula $Li_{1.6}Na_{0.4}TiM(PO_4)_3$ (M = Fe, Cr), highlighting the presence of remaining sodium ions. Contrary to the pure sodium compositions, the space group is unambiguously $R\bar{3}$ rather than $R\bar{3}c$. Indeed, the XRD patterns of Figure 1 clearly show reflections such as (303) ($2\theta_{CoK\alpha} \approx 46°$) which is normally forbidden in the $R\bar{3}c$ space

(18) Shannon, R. D. *Acta Crystallogr.* **1976**, *A32*, 751−767.
(19) Masquelier, C.; Wurm, C.; Rodrìguez-Carvajal, J.; Gaubicher, J.; Nazar, L. *Chem. Mater.* **2000**, *15*, 525−532.

Table 2. Atomic Coordinates of B−$Na_2TiFe(PO_4)_3$ (A) and B−$Na_2TiCr(PO_4)_3$ (B)[a]

(A) Atomic Coordinates of B−$Na_2TiFe(PO_4)_3$

atom	sites	*x*	*y*	*z*	B_{eq} (Å^2)	occ.
Na(1)	*6b*	0	0	0	[b]	0.98(1)
Na(2)	*18e*	0.6334(13)	0	0.25	[b]	0.34(1)
Fe	*12c*	0	0	0.1466(2)[c]	0.51(9)	0.5
Ti	*12c*	0	0	0.1466(2)[c]	0.51(9)	0.5
P	*18e*	0.2900(2)	0	0.25	0.47(5)	1
O(1)	*36f*	0.1780(2)	−0.0239(2)	0.1930(1)	1.46(4)	1
O(2)	*36f*	0.3090(2)	−0.1673(2)	0.2548(1)	0.75(3)	1

atom	β_{11}	β_{22}	β_{33}	β_{12}	β_{13}	β_{23}
Na(1)	286(27)	286(27)	1(1)	143(27)	0	0
Na(2)	5(2)	5(2)	29(3)	3(2)	8(2)	17(2)

(B) Atomic Coordinates of B−$Na_2TiCr(PO_4)_3$

atom	sites	*x*	*y*	*z*	B_{eq} (Å^2)	occ.
Na(1)	*6b*	0	0	0	[b]	0.96(1)
Na(2)	*18e*	0.6355(15)	0	0.25	1.13(25)	0.35(1)
Cr	*12c*	0	0	0.1480(2)[c]	0.7	0.5
Ti	*12c*	0	0	0.1480(2)[c]	0.7	0.5
P	*18e*	0.2890(3)	0	0.25	0.94(5)	1
O(1)	*36f*	0.1750(3)	−0.0263(2)	0.1930(1)	1.53(4)	1
O(2)	*36f*	0.3071(2)	−0.1691(2)	0.2559(1)	0.83(3)	1

atom	β_{11}	β_{22}	β_{33}	β_{12}	β_{13}	β_{23}
Na(1)	339(35)	339(35)	1(1)	170(35)	0	0

[a] ESDs are given in parentheses. Equivalent thermal displacement parameters (B_{eq}) such as $B_{eq} = (8\pi^2/3)\sum_i\sum_j U_{ij}\cdot a_i^*\cdot a_j^*\cdot a_i\cdot a_j$, and anisotropic thermal displacements of Na(1) ions are also given. [b] Refined anisotopically. [c] Constrained.

Table 3. Selected Bond Lengths (Å) with Standard Deviation in Parentheses and Average Distances (⟨X−O⟩) for (A) B−$Na_2TiFe(PO_4)_3$ and B−$Na_2TiCr(PO_4)_3$ and (B) B−$Li_{1.6}Na_{0.4}TiFe(PO_4)_3$ and B−$Li_{1.6}Na_{0.4}TiCr(PO_4)_3$

	B−$Na_2TiFe(PO_4)_3$	B−$Na_2TiCr(PO_4)_3$
$Na(1)O_6$	⟨2.4584⟩	⟨2.4677⟩
	6 * 2.4584 (O(2))	6 * 2.4677 (O(2))
$Na(2)O_8$	⟨2.5535⟩	⟨2.5424⟩
	2 * 2.8381 (O(1))	2 * 2.7962 (O(1))
	2 * 2.6196 (O(1))	2 * 2.6249 (O(1))
	2 * 2.4196 (O(2))	2 * 2.4396 (O(2))
	2 * 2.3367 (O(2))	2 * 2.3087 (O(2))
MO_6 (M = Ti, Fe, Cr)	⟨1.9634⟩	⟨1.9426⟩
	3 * 1.9284 (O(1))	3 * 1.8937 (O(1))
	3 * 1.9984 (O(2))	3 * 1.9914 (O(2))
PO_4	⟨1.5247⟩	⟨1.5286⟩
	2 * 1.5184 (O(1))	2 * 1.5204 (O(1))
	2 * 1.5310 (O(2))	2 * 1.5368 (O(2))
	B−$Li_{1.6}Na_{0.4}TiFe(PO_4)_3$	B− $Li_{1.6}Na_{0.4}TiCr(PO_4)_3$
LiO_4	⟨2.0127⟩	⟨2.1190⟩
	1 * 1.6170 (O(1′))	1 * 2.0970 (O(1′))
	1 * 1.8026 (O(2))	1 * 2.3611 (O(1′))
	1 * 2.3318 (O(2))	1 * 2.0647 (O(2))
	1 * 2.2994 (O(2′))	1 * 1.9531 (O(2′))
$Na(1a)O_6$	⟨2.4688⟩	⟨2.4770⟩
	6 * 2.4688 (O(2′))	6 * 2.4770 (O(2′))
$Na(1b)O_6$	⟨2.6439⟩	⟨2.6235⟩
	6 * 2.6439 (O(2))	6 * 2.6235 (O(2))
$M(1)O_6$ (M = Ti, Fe, Cr)	⟨1.9439⟩	⟨1.9498⟩
	3 * 1.9080 (O(1))	3 * 1.9142 (O(1))
	3 * 1.9799 (O(2′))	3 * 1.9854 (O(2′))
$M(2)O_6$ (M = Ti, Fe, Cr)	⟨1.9474⟩	⟨1.9453⟩
	3* 1.8757 (O(1′))	3* 1.8050 (O(1′))
	3 * 2.0191 (O(2))	3 * 2.0856 (O(2))
PO_4	⟨1.5297⟩	⟨1.5296⟩
	1 * 1.5522 (O(1))	1 * 1.4675 (O(1))
	1 * 1.5029 (O(1′))	1 * 1.5719 (O(1′))
	1 * 1.5550 (O(2))	1 * 1.5891 (O(2))
	1 * 1.5088 (O(2′))	1 * 1.4901 (O(2′))

group. The cell parameters are $a = 8.390(1)$ Å and $c = 22.040(3)$ Å for B−$Li_{1.6}Na_{0.4}TiFe(PO_4)_3$; and $a = 8.342(1)$ Å and $c = 21.951(2)$ Å for B−$Li_{1.6}Na_{0.4}TiCr(PO_4)_3$ (Table 1).

The refinement of the $[MTi(PO_4)_3]$ framework atomic coordinates was conducted as for B−$Na_2TiM(PO_4)_3$, with the exception that the change of space group (from $R\bar{3}c$ to $R\bar{3}$) doubles the number of M, Ti, and O sites (i.e., divides the multiplicity of the sites by two). The location of the alkali cations within the framework remained to be determined, and many possibilities to distribute 0.4 Na^+ and 1.6 Li^+ between the three possible sites

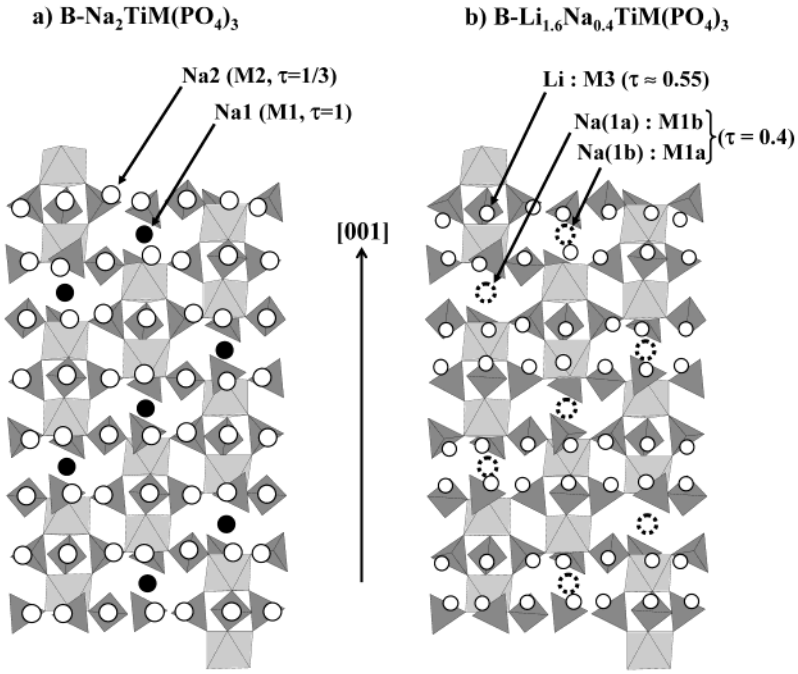

Figure 3. (a) Structure of B−$Na_2TiM(PO_4)_3$ (M = Fe, Cr) viewed along [001]. (b) Structure of B−$Li_{1.6}Na_{0.4}TiM(PO_4)_3$ (M = Fe, Cr) viewed along [001].

(usually labeled M1, M2, and M3) were tested. The best refinements were obtained by placing the lithium ions in a single 4-coordinated M3 site (*18f*) and the sodium ions in the 6-coordinated M1 site, which is split into M1a and M1b (*3a* and *3b*, respectively) (Figure 3). In these conditions the 8-coordinated M2 sites are empty. As already mentioned by one of us,[19] the smaller size of Li^+ compared to Na^+ favors the occupancy of a 4-coordinated site (M3) for lithium rather than an 8-coordinated site (M2). Table 1 indicates a significant increase (∼4%) of the *c*/*a* ratio when Li^+ is substituted for Na^+, which is a clear signature of partial depopulation of the M1 site. The atomic coordinates are summarized in Table 4a and b for both iron and chromium materials, and selected bond lengths are given in Table 3b. In the case of B−$Li_{1.6}Na_{0.4}TiFe(PO_4)_3$, thermal displacement factors of lithium are highly anisotropic ($\beta_{11} \gg \beta_{22}$ and β_{33}). Unfortunately, this trend could not been confirmed in the refinement of B−$Li_{1.6}Na_{0.4}TiCr(PO_4)_3$, because we had to constrain some parameters equal, such as the isotropic thermal displacement factors of Li and Na (we recall that *b*(Ti) ∼ −*b*(Cr)). Again, distances (Table 3b), angles, bond strengths, and polyhedra distortions calculations confirmed the validity of both structures.

Figure 4 gathers the values of the *c*/*a* ratio for an extensive series of NASICON compositions $Z_xMM'(PO_4)_3$ containing various amounts (*x*) of lithium or sodium ($TiNb(PO_4)_3$, $ZTi_2(PO_4)_3$, $ZFeNb(PO_4)_3$, $Z_2TiCr(PO_4)_3$, $Z_2TiFe(PO_4)_3$, $Z_3Fe_2(PO_4)_3$, $Z_3FeCr(PO_4)_3$, and $Z_3Cr_2(PO_4)_3$, Z = Li, Na; $0 \le x \le 3$). The *c*/*a* ratio is strongly correlated to the occupancy of the M1 site by lithium or sodium.[20] As *c* increases, *a* decreases through a relaxation phenomenon, when M1 is emptied.

For the sodium-containing compositions, increasing *x* corresponds to a progressive filling of the M2 site while the M1 site remains fully occupied. This generates an increase of *a* while *c* remains almost constant, hence a decrease of *c*/*a*.

For lithium-containing compositions, increasing *x* corresponds to a depopulation of the M1 site. It is completely filled for $LiFeNb(PO_4)_3$ and $LiTi_2(PO_4)_3$, and completely empty for $Li_3MM'(PO_4)_3$ (M, M′ = Fe, Cr)[19,21−22]. This generates a strong increase of **c** while **a** remains almost constant, hence an increase of *c*/*a*. As mentioned, both "$Li_2TiCr(PO_4)_3$" and "$Li_2TiFe(PO_4)_3$" still contain 0.4 sodium ions inside their M1 site, which tends to locate the *c*/*a* ratio at intermediate values.

3. Electrochemical Insertion of Lithium or Sodium. Electrochemical activity toward lithium or sodium insertion is observed for the four compositions of this study ($Li_2TiM(PO_4)_3$ and $Na_2TiM(PO_4)_3$ (M = Fe, Cr)), thanks to the presence of Ti^{4+} and Fe^{3+}, which can be reduced into Ti^{3+} and Fe^{2+}. With no surprise, only one electron per formula unit could be exchanged for the mixed Ti/Cr materials as a direct consequence of the electrochemical inactivity of chromium in the range of potentials we studied (3.4−2.0 V vs Li^+/Li, 3.1−1.7 V vs Na^+/Na). On the contrary, both Ti/Fe materials exchanged two electrons per formula unit.

3a. Electrochemical Insertion of Lithium into $Li_{1.6}Na_{0.4}TiM(PO_4)_3$. Figure 5 shows the electrochemical data recorded during lithium insertion into $Li_{1.6}Na_{0.4}TiFe(PO_4)_3$ and $Li_{1.6}Na_{0.4}TiCr(PO_4)_3$, in GITT mode. As deduced from the GITT experiments and from "derivative" curves ($-\partial x/\partial U = f(U)$) of $Li_{1.6}Na_{0.4}TiCr(PO_4)_3$ (not shown here), we determined that the average potential of the $Ti^{4+/3+}$ redox couple was located at 2.55 V vs Li^+/Li. This is consistent with the data of $Li_{1.6}Na_{0.4}TiFe$-

(20) Wurm, C. Ph.D. Thesis, Université de Paris-Sud, 2002. Cherkaoui, F. Ph.D. Thesis, Université de Bordeaux I, 1985.

(21) Aatiq, A.; Delmas, C.; El Jazouli, A. *J. Solid State Chem.* **2001**, *158*, 169−174.

(22) Aatiq, A.; Delmas, C.; El Jazouli, A.; Gravereau, P. *Ann. Chim. Sci. Mater.* **1998**, *23*, 121−124.

Table 4. Atomic Coordinates of B−$Li_{1.6}Na_{0.4}TiFe(PO_4)_3$ (A) and B−$Li_{1.6}Na_{0.4}TiCr(PO_4)_3$ (B)

(A) Atomic Coordinates of B−$Li_{1.6}Na_{0.4}TiFe(PO_4)_3$

atom	sites	*x*	*y*	*z*	B_{eq} (Å^2)	occ.
Li	*18f*	0.279(8)	0.046(3)	0.372(2)	a	0.54(1)
Na(1a)	*3a*	0	0	0	2.68(62)	0.60(1)
Na(1b)	*3b*	0	0	0.5	5.46(99)	0.26(1)
Fe(1)	*6c*	0	0	0.1440(8)[c]	1.39(22)[d′]	0.50(1)
Ti(1)	*6c*	0	0	0.1440(8)[c]	1.39(22)[d′]	0.50(1)
Fe(2)	6c	0	0	0.6527(8)[d]	1.77(24)[e′]	0.50(1)
Ti(2)	*6c*	0	0	0.6527(8)[d]	1.77(24)[e′]	0.50(1)
P	*18f*	0.2893(6)	0.0044(7)	0.2514(3)	1.60(7)	1
O(1)	*18f*	0.1853(9)	−0.0089(7)	0.1916(2)	3.25(11)	1
O(1′)	*18f*	0.7840(8)	0.9389(6)	0.6957(2)	3.13(10)	1
O(2)	*18f*	0.2611(6)	−0.1911(7)	0.2627(2)	2.56(9)	1
O(2′)	*18f*	0.5081(7)	0.8578(7)	0.7542(2)	2.28(9)	1

atom	β_{11}	β_{22}	β_{33}	β_{12}	β_{13}	β_{23}
Li	3339(431)	109(53)	326(51)	754(143)	1149(134)	286(43)

(B) Atomic Coordinates of B−$Li_{1.6}Na_{0.4}TiCr(PO_4)_3$

atom	sites	*x*	*y*	*z*	B_{eq} (Å^2)	occ.
Li	*18f*	0.347(1)	0.066(2)	0.388(1)	0.62(37)[c]	0.55(1)
Na(1a)	*3a*	0	0	0	0.62(37)[c]	0.36(1)
Na(1b)	*3b*	0	0	0.5	0.62(37)[c]	0.32(1)
Cr(1)	*6c*	0	0	0.143(3)[d]	0.7	0.5
Ti(1)	*6c*	0	0	0.143(3)[d]	0.7	0.5
Cr(2)	*6c*	0	0	0.654(3)[d′]	0.7	0.5
Ti(2)	*6c*	0	0	0.654(3)[d′]	0.7	0.5
P	*18f*	0.2854(6)	0.0020(7)	0.2485(3)	0.92(9)	1
O(1)	*18f*	0.1843(10)	−0.0088(7)	0.1925(2)	2.80(14)	1
O(1′)	*18f*	0.7792(8)	0.9307(7)	0.6945(2)	2.16(12)	1
O(2)	*18f*	0.2562(7)	−0.1975(7)	0.2628(2)	1.87(11)	1
O(2′)	*18f*	0.5125(7)	0.8620(7)	0.7541(2)	0.87(10)	1

[a] ESDs are given in parentheses. Equivalent thermal displacement parameters (B_{eq}), such as $B_{eq} = (8\pi^2/3)\sum_i\sum_j U_{ij}\cdot a_i^*\cdot a_j^*\cdot a_i\cdot a_j$ *and anisotropic thermal displacements of lithium ions are also given.* [b] Refined anisotopically. [c,c′,d,d′] Constrained.

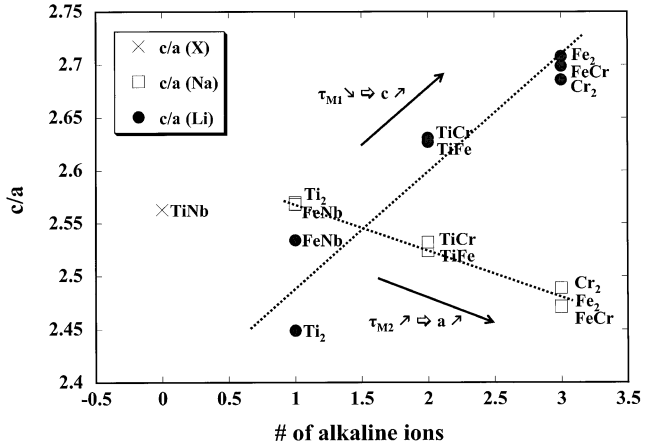

Figure 4. Schematic representation of the *c*/*a* ratio in NASICON structure, depending on the alkaline ions and their amount.

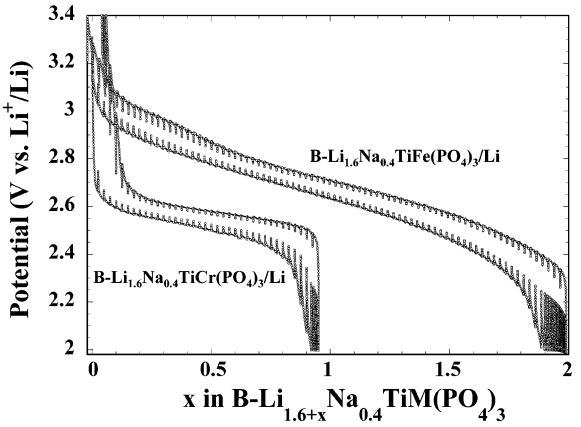

Figure 5. Potential−composition curves vs Li^+/Li of B−$Li_{1.6}Na_{0.4}TiFe(PO_4)_3$ and B−$Li_{1.6}Na_{0.4}TiCr(PO_4)_3$, performed in a galvanostatic intermittent mode (GITT): regime of C/20 for 30 min and relax periods of 30 min.

$(PO_4)_3$, where the Ti^{4+}/Ti^{3+} redox couple is lower than the average potential of Fe^{3+}/Fe^{2+} (2.80−2.85 V vs Li^+/Li). Such potentials are in good agreement with those reported by Aatiq for $Ti^{4+/3+}$ in NASICON $LiTi_2(PO_4)_3$ and $Li_{0.5}Mn_{0.5}Ti_{1.5}Cr_{0.5}(PO_4)_3$[21,22] and our group[23] for $Fe^{3+/2+}$ in NASICON $Li_3Fe_2(PO_4)_3$.

PITT measurements of both materials were performed to detect the presence of single- or two-phase domains, and to give information on the factors limiting the transformations. For B−$Li_{1.6}Na_{0.4}TiCr(PO_4)_3$, the shape of current decays (recorded in PITT mode) is similar to that observed for B−$Li_{1.6}Na_{0.4}TiFe(PO_4)_3$ (Figure 6). Such current decays are similar in both charge and discharge (Figure 7) and strongly suggest a solid solution process for the whole intercalation range. The shape of these current decays denotes a kinetic limitation of the electron transport inside the material rather than a lithium diffusion limitation (front-phase migration). We also found a single-phase process for the insertion of lithium into A-$Li_2TiM(PO_4)_3$[12] which is in contrast with $LiTi_2(PO_4)_3/Li_3Ti_2(PO_4)_3$[24,25] and B−$Li_{3+x}Fe_2(PO_4)_3$ ($0 \le x \le 2$),[23,26] which present obvious or complex two-phase processes, respectively. One expla-

(23) Morcrette, M.; Wurm, C.; Masquelier, C. *Solid State Sci.* **2002**, *4*, 239−246.

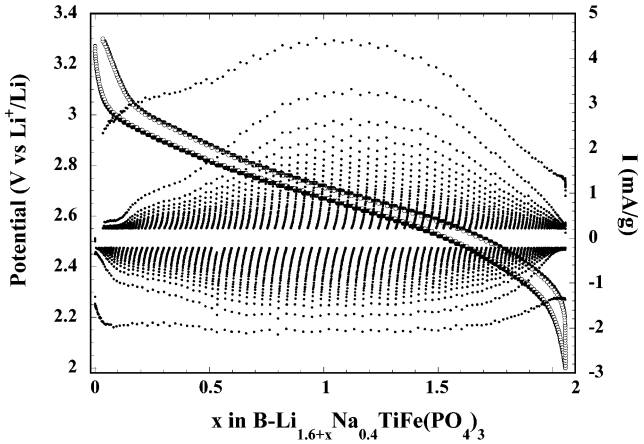

Figure 6. Potentiometric titration curve (PITT) of B−$Li_{1.6}$-$Na_{0.4}TiFe(PO_4)_3$ in the 3.4−2.0 V range vs Li^+/Li (i_{min} = 3.5 μA, equivalent to a C/300 regime).

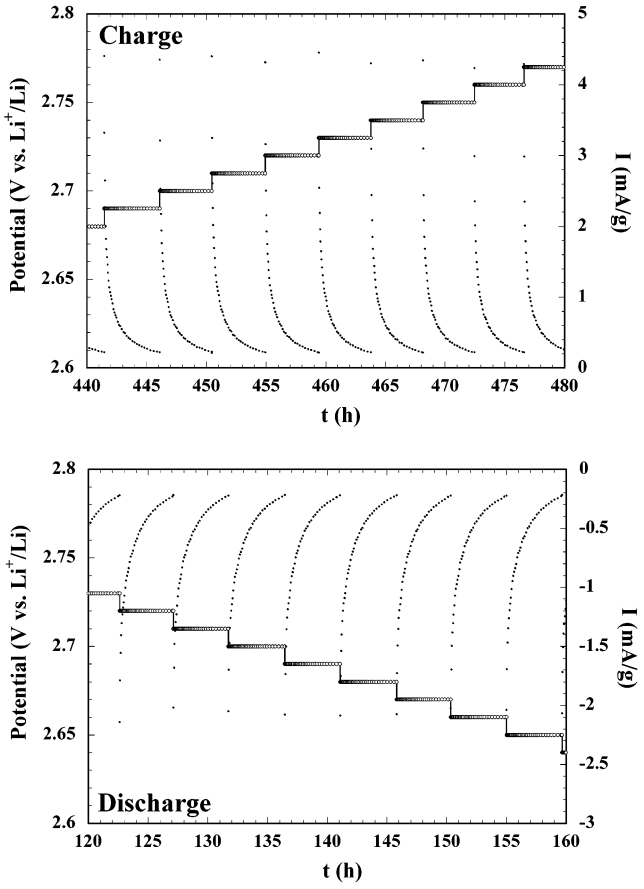

Figure 7. Zoom of the PITT curve of B−$Li_{1.6}Na_{0.4}TiFe(PO_4)_3$ (Figure 6) showing the current decays in charge and discharge for the same values of *x*.

nation to these peculiar features of orthorhombic and rhombohedral $Li_2TiM(PO_4)_3$ could be nested in the structural disorder of Ti and M into the framework.

To get more insight into the conclusions arising from the PITT measurements, *in situ* X-ray diffraction studies during lithium insertion into both B−$Li_{1.6}Na_{0.4}$TiM-

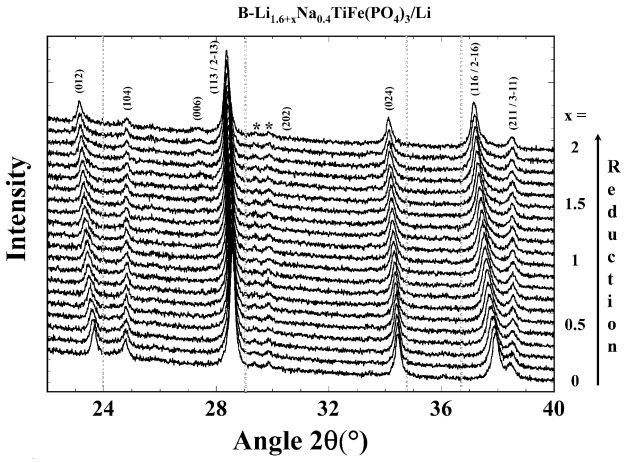

Figure 8. Evolution of the *in situ* X-ray diffraction patterns of an electrode of B−$Li_{1.6}Na_{0.4}TiFe(PO_4)_3$ during the insertion of lithium, under a GITT mode in the 3.4−2.0 V range vs Li^+/Li. Acquisition time of 1 h in the 15.00−45.00 2θ (°) angular range from Co Kα radiation on a D8-Bruker diffractometer equipped with a PSD counter.

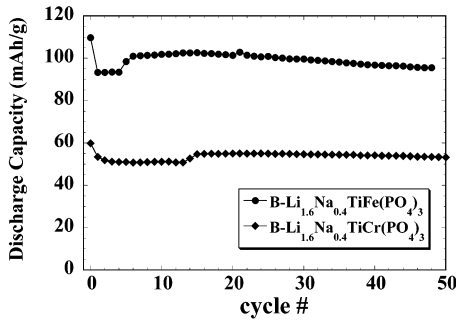

Figure 9. Specific capacity (in discharge) vs cycle no. of B−$Li_{1.6}Na_{0.4}TiM(PO_4)_3$ (M = Fe, Cr) under a C/10 cycling rate.

$(PO_4)_3$ (M = Fe, Cr) compounds were performed. Both materials present similar trends and we report here only the data relavant to the B−$Li_{1.6}Na_{0.4}TiFe(PO_4)_3$/Li system (Figure 8). As indicated by the continuous shift of all the diffraction peaks (no change of space group) on lithium insertion, *in situ* XRD confirms the solid-solution process evocated from the PITT data. The high reversibility of the system was also confirmed (not presented). This generates very stable capacity retention on cycling (~100 mAh/g for $Li_{1.6}Na_{0.4}TiFe(PO_4)_3$ and 50 mAh/g for $Li_{1.6}Na_{0.4}TiCr(PO_4)_3$), as shown on Figure 9. Data extracted from full-pattern refinements of all the *in situ* XRD patterns will be discussed in detail in Section 3c.

3b. Electrochemical Insertion of Sodium into $Na_2TiM(PO_4)_3$. Both $Na_2TiFe(PO_4)_3$ and $Na_2TiCr(PO_4)_3$ reversibly insert sodium with very small internal impedance, as shown in Figure 10. As for $Li_{1.6}Na_{0.4}TiM(PO_4)_3$/Li, the extreme compositions $Na_4TiFe(PO_4)_3$ and $Na_3TiCr(PO_4)_3$ correspond to the complete reduction of Fe^{3+} into Fe^{2+} and Ti^{4+} into Ti^{3+}. $Na_2TiFe(PO_4)_3$ and $Na_2TiCr(PO_4)_3$ being isostructural, it is legitimate to attribute the first half ($2 \le x \le 3$) of the electrochemical curve of $Na_xTiFe(PO_4)_3$ to the Fe^{3+}/Fe^{2+} redox couple, hence located at 2.4 V vs Na^+/Na (average potential). The second half ($3 \le x \le 4$) corresponds to the Ti^{4+}/Ti^{3+} redox couple, located at 2.20−2.15 V vs Na^+/Na (average potential). It lies at the same value as $Na_xTiCr(PO_4)_3$

(24) Delmas, C.; Nadiri, A.; Soubeyroux, J. L. *Solid State Ionics* **1988**, *28*−*30*, 419−423.
(25) Patoux, S.; Masquelier, C. *Chem. Mater.* **2002**, *14*, 5057−5068.
(26) Anderson, A. S.; Kalska, B.; Eyob, P.; Aernout, D.; Häggström,L.; Thomas, J. O. *Solid State Ionics* **2001**, *140*, 63−70.

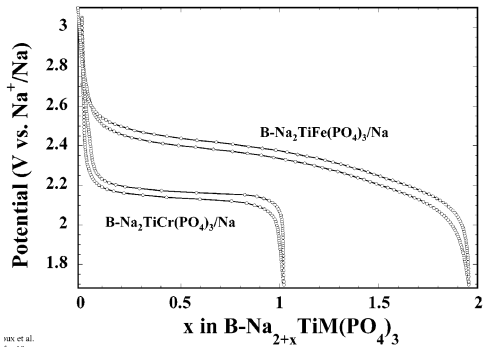

Figure 10. Potential−composition curves vs Na^+/Na of $B-Na_2TiFe(PO_4)_3$ and $B-Na_2TiCr(PO_4)_3$, performed in a galvanostatic mode (regime of C/10).

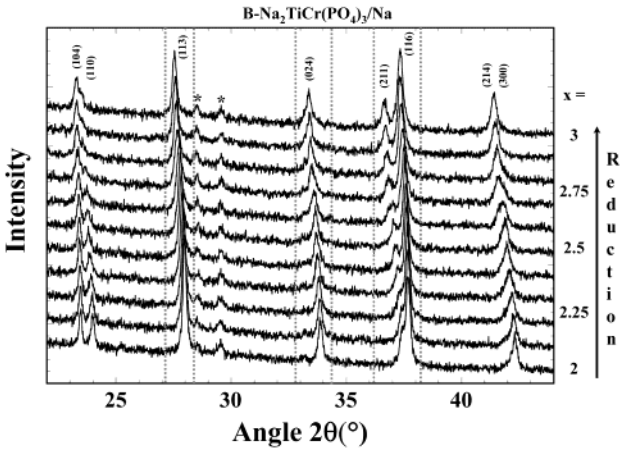

Figure 11. Evolution of the *in situ* X-ray diffraction patterns of an electrode of $B-Na_2TiCr(PO_4)_3$ during the insertion of sodium, under a GITT mode in the 3.1−1.7 V range vs Na^+/Na. Acquisition time of 1 h in the 15.00−45.00 2θ(°) angular range from a Co Kα radiation on a D8 Bruker diffractometer equipped with a PSD counter. Asterisks denote contributions from the cell hardware.

($2 \le x \le 3$). Note that the values of the potentials of the Fe^{3+}/Fe^{2+} and Ti^{4+}/Ti^{3+} redox couples are basically unchanged for Na^+ or Li^+ insertion: the experimental cell voltage difference (0.3−0.4 V) is directly related to the difference of potential between the Na^+/Na and Li^+/Li couples.

Tillement[9] attributed a nearly horizontal plateau on discharge of a $Na_2TiFe(PO_4)_3/Na$ cell to a two-phase region between $Na_2TiFe(PO_4)_3$ and $Na_{2.5}TiFe(PO_4)_3$ which could be the result of a stabilized local configuration of alkali cations for $Na_{2.5}TiFe(PO_4)_3$ into which half of the M2 sites would be filled (τ_{M1} remaining equal to 1). Our data indicate that electrochemical insertion of Na^+ into $Na_2TiFe(PO_4)_3$ and $Na_2TiCr(PO_4)_3$ proceeds as single-phase reactions all along the insertion domain. This is supported by the shapes of the current decay in PITT mode that are typical of solid solution reactions, similarly to what we presented for $B-Li_{1.6}Na_{0.4}TiFe(PO_4)_3$. It is also consistent with the continuous shift of the diffraction peaks of the *in situ* XRD patterns during reduction of $Na_2TiCr(PO_4)_3$ down to 1.7 V vs Na^+/Na (Figure 11).

3c. Anisotropic Lattice Expansion/Extraction during Lithium or Sodium Insertion. Figure 12 retraces the evolution of the **a** and **c** unit-cell parameters, as well as the *c*/*a* ratio and volume, during electrochemical

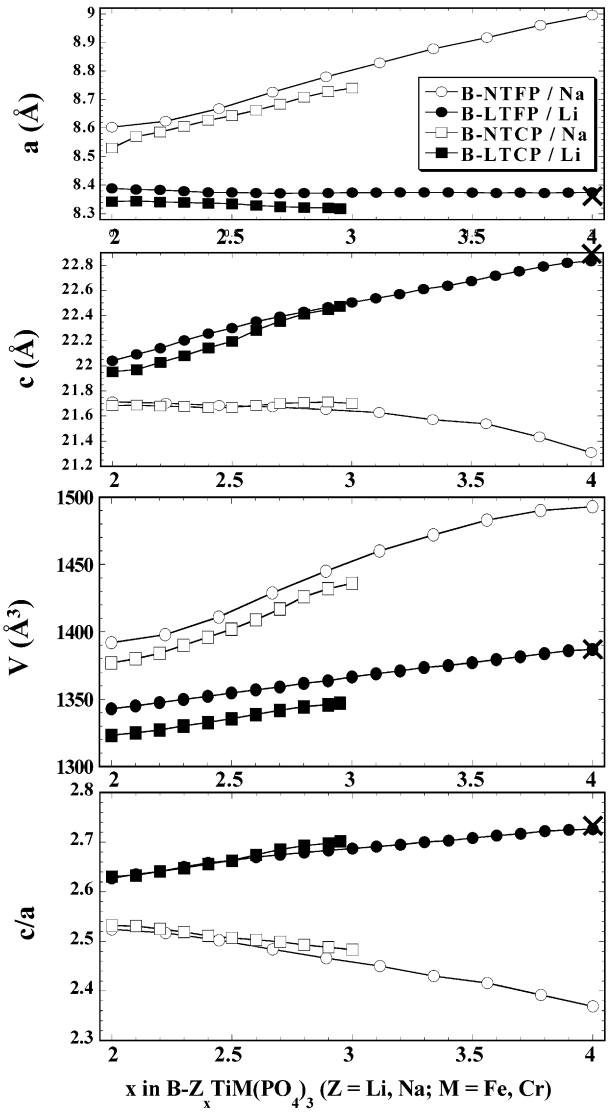

Figure 12. Lattice parameters (*a*, *c*, *V*, and *c*/*a*) expansions of $B-Na_xTiM(PO_4)_3$ and $B-Li_{1.6}Na_{0.4}TiM(PO_4)_3$ ($2 < x < 3$ for M = Cr and $2 < x < 4$ for M = Fe) during the first reduction, deducted from the *in situ* data between 3.4 and 2.0 V vs Li^+/Li and between 3.1 and 1.7 V vs Na^+/Na. The cross symbols indicate the values obtained on $B-Li_{3.6}Na_{0.4}TiFe(PO_4)_3$ prepared by chemical lithiation.

insertion of lithium or sodium into $B-Z_2TiM(PO_4)_3$ (Z = Li, Na; M = Fe, Cr). Each of the four materials will be labeled with 4 letters, such as LTFP for $Li_2TiFe(PO_4)_3$ for instance.

The increase in ionic radii[18] of titanium ($r_{Ti4+} = 0.605$ Å; $r_{Ti3+} = 0.670$ Å) and iron ($r_{Fe3+} = 0.645$ Å; $r_{Fe2+} = 0.78$ Å) ions during alkali ion insertion, tends to globally increase the unit-cell volume. For both lithium and sodium insertion, mixed Ti/Fe materials display a stronger volume expansion than the mixed Ti/Cr materials, as only one electron per formula unit was exchanged in the latter case (smaller amount of inserted species). The general trend (slope $\delta V/\delta x$) is similar though. The overall lattice expansions for the four compositions investigated here are the following: +7.26, +4.28, +3.27, and +2.70% for NTFP, NTCP, LTFP, and LTCP, respectively. It appears then that the unit-cell expansion is higher during sodium insertion than during lithium insertion. This behavior is not as trivial as

it appears and we found that anisotropic variations of the *a* and *c* parameters depended on the nature of the alkali ion inserted itself.

To account for these observations, it is interesting to recall the extensive literature on NASICON compositions that had been investigated in the 1980s and for which sodium distribution over various interstitial sites within the framework was a major parameter to be related with ionic conductivity. For instance, the compositions $Na_{1+x}Zr_{2-x}L_x(PO_4)_3$ (L = Cr, In, Yb; $0 \le x \le 2$)[27] and $Na_{1+x}Zr_{2-x/2}Mg_{x/2}(PO_4)_3$ ($0 \le x \le 2$)[28] were studied in detail by Delmas. Note that the amount $(1 + x)$ of sodium was fixed by substituting given amounts of Zr^{4+} by L^{3+} or Mg^{2+}, and not by electrochemical insertion.

It is well-established that the value of the **a**-parameter is strongly correlated to the following: the size of the M and M′ cations of the $[MM'(PO_4)_3]$ framework, as MO_6 and $M'O_6$ octahedra form some sort of ribbons in the (**a**, **b**) plane, and the amount of alkaline ions inside these ribbons (M2 sites).

Even better established is that the value of the *c*-parameter is strongly correlated to the occupation rate of the M1 site (located halfway between $[MM'(PO_4)_3]$ units along [001]), the "positive" charge on M and M′, and their size.

During lithium insertion, both LTFP and LTCP show a decrease in the **a**-parameter (−0.17% and −0.29%, respectively), whereas **c** strongly increases (+3.60% and +2.37%, respectively). This is clearly illustrated in Figure 8 by the large shift of the (116) peak around 37−38 2θ(°). As a result, the *c*/*a* ratio increased by +3.77% for LTFP and by +2.70% for LTCP. From the considerations given above, we propose that the anisotropic elongation of the LTFP and LTCP cells along [001] during Li insertion might be induced by a progressive transfer of the 0.4 remaining sodium from the M1 to the M2 sites, by the increase of transition metal ionic radii as *x* increases, and by the progressive filling of the M3 site by lithium, as for $Li_{3+x}Fe_2(PO_4)_3$.[29] The much weaker variation of **a** (decrease) is probably accounted for by a relaxation phenomenon of the framework.

The end-member, reduced composition $Li_{3.6}Na_{0.4}TiFe(PO_4)_3$ was also prepared from the parent $Li_{1.6}Na_{0.4}TiFe(PO_4)_3$ by chemical lithiation with *n*-butyllithium, in hexane solution. After a 7-day immersion under magnetic stirring, the powder was washed 4× in clean hexane solutions, and dried under vacuum for several hours. Because of air and moisture sensitivity, the obtained $Li_{3.6}Na_{0.4}TiFe(PO_4)_3$ powder was kept in an argon-filled drybox. An X-ray diffraction pattern was collected for 4.5 h, with the sample being placed within the same cell as for the *in situ* experiments. The XRD pattern is provided in Figure 13 and compared with that obtained during the *in situ* experiment. The Bragg positions corresponding to an $a = 8.363(1)$ Å; $c = 22.882(3)$ Å ($V = 1386(1)$ Å^3) unit-cell in the $R\bar{3}$ space group are also drawn. Both data are very consistent.

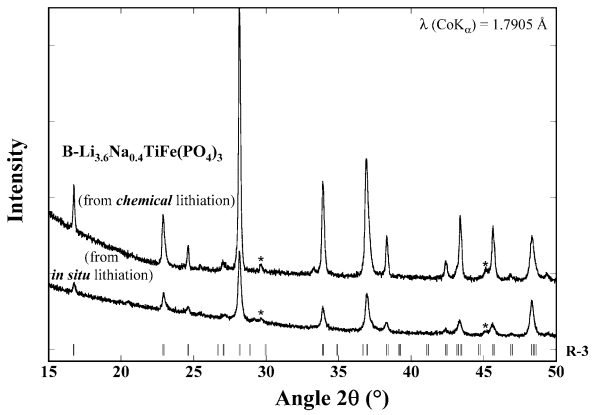

Figure 13. X-ray diffraction patterns collected at 300 K on a D8 Bruker diffractometer (Co Kα radiation, $\lambda = 1.7905$ Å, $\theta-\theta$ geometry, back monochromator) of $B-Li_{3.6}Na_{0.4}TiFe(PO_4)_3$ prepared by chemical lithiation or electrochemical reduction. The Bragg positions calculated in the space group $R\bar{3}$ with $a = 8.363$ Å and $c = 22.882$ Å are also reported. Asterisks denote contributions from the cell hardware.

The complete structural study of $B-Li_{3.6}Na_{0.4}TiFe(PO_4)_3$ through powder neutron diffraction is scheduled for the near future and will probably allow determination of the exact location of Li (and remaining Na) ions within the interstitial space of the NASICON framework.

During sodium insertion, however, both NTFP and NTCP show a large increase in the **a**-parameter by +4.56 and +2.07% (shift of the (211) peak around 37 2θ(°) in Figure 11), whereas **c** smoothly decreases by −1.86 and ∼0%, respectively. Consequently, the *c*/*a* ratio decreases by −6.14% for NTFP and by −1.94% for NTCP. The strong increase in the **a**-parameter would be attributed to the filling of the M2 sites, added to the increase in the ionic radii. This is consistent with the results of Tillement on $Na_xZrFe(PO_4)_3$ ($2 \le x \le 3$),[30] into which zirconium is not electrochemically active and iron is reduced to Fe^{2+}.

Conclusion

We presented the crystal structures of NASICON $Na_2TiM(PO_4)_3$ ($R\bar{3}c$) and $Li_{1.6}Na_{0.4}TiM(PO_4)_3$ ($R\bar{3}$) (M = Fe, Cr) from neutron diffraction experiments. The $[TiM(PO_4)_3]$ units are similar, and the main changes are nested in the alkaline ions distributions among three possible sites. This study also demonstrates the exceptional stability of the NASICON framework toward reversible insertion/extraction of sodium or lithium, particularly true when *x* is between $x = 2$ and $x = 4$ in $Z_xMM'(PO_4)_3$. Remarkably, the four compositions of this study all show very small polarization during charge or discharge and full theoretical capacity is reached experimentally. This capacity is small in the case of Cr-containing $Z_xTiCr(PO_4)_3$ ($2 \le x \le 3$) as Cr^{3+} is not reduced, whereas the capacity observed for $Z_xTiFe(PO_4)_3$ ($2 \le x \le 4$) is twice as important.

For mixed $Z_xTiM(PO_4)_3$ (Z = Na, Li and M = Fe, Cr) compositions, we demonstrated that, for both Li^+ and Na^+ insertion, the mechanism involved was a single-phase process during the whole insertion range ($2 \le x$

(27) Delmas, C.; Viala, J.-C.; Olazcuaga, R.; Le Flem, G.; Hagenmuller, P.; Cherkaoui, F.; Brochu, R. *Solid State Ionics* **1981**, *3/4*, 209−214.

(28) Cherkaoui, F.; Viala, J. C.; Delmas, C.; Hagenmuller, P. *Solid State Ionics* **1986**, *21*, 333−337.

(29) Eyob, P.; Anderson, A. S.; Thomas, J. O. *J. Mater. Chem.* **2002**, *12*, 1−6.

(30) Tillement, O.; Angenault, J.; Couturier, J. C.; Quarton, M. *Solid State Ionics* **1991**, *44*, 299−203.

≤ 4 and $2 \leq x \leq 3$, for M = Fe and Cr, respectively). This is in contrast with the NASICON compositions $Z_xTi_2(PO_4)_3$ ($1 \leq x \leq 3$) and $Z_xFe_2(PO_4)_3$ ($3 \leq x \leq 5$), which show two-phase insertion/deinsertion plateaus all along the composition ranges, even if the situation is a little more complex for $Li_3Fe_2(PO_4)_3$. We discussed the change of the lattice parameters during insertion, and showed that the general skeletons seemed to be maintained. Once again, the changes of lattice properties are governed by the nature of alkaline ions, their distribution and their amount.

Acknowledgment. We are grateful to M. Morcrette for challenging discussions and help in designing the *in situ* XRD equipment, to J.-M. Tarascon for his support and critical review of the manuscript, and to M. Nelson for corrections of the English grammar.

Supporting Information Available: Crystallographic data for the subject structures (W.C.). This material is available free of charge via the Internet at http://pubs.acs.org.

CM020479P